

Analysis of Focusing of Pulsed Baseband Signals Inside a Layered Tissue Medium

Konstantina S. Nikita, *Member, IEEE*, Georgios D. Mitsis, and Nikolaos K. Uzunoglu, *Senior Member, IEEE*

Abstract—The derivation and application of a method designed to investigate the focusing properties of pulsed baseband signals of short pulsewidth (~ 1 ns) in biological tissue media are reported. To this end, sources fed from TEM waveguides, concentrically placed at the periphery of a three-layer cylindrical lossy model, are assumed. A Fourier-series-based methodology, appropriate for a useful class of pulse train incident signals, is presented and utilized to study the dynamics of pulse propagation inside the tissue medium. The propagation of each spectral component of the incident field within the tissue medium is analyzed by applying an integral-equation technique and a Fourier-series representation is used in order to obtain the time dependence of the electromagnetic fields produced at any point within tissue due to the pulsed excitation of the array elements. Numerical results are computed and presented at several points in a three-layer geometry, 20 cm in diameter, irradiated by an eight-element waveguide array. Focusing at a specific point of interest within tissue is achieved by properly adjusting the time delay of the signals injected to the individual applicators of the array.

Index Terms—Biological tissues, focusing, pulsed signals.

I. INTRODUCTION

THE principle idea of using positive interference arising from various near- or far-field sources to create focusing of electromagnetic waves has extensively been employed during the past 50 years based on the use of continuous wave signals. In this context, phased-array principles and optimization techniques have been applied to develop hyperthermia systems for the treatment of malignant tumors [1]–[3]. The main limitations of continuous wave concepts used to achieve focusing have been related to the excessive loss suffered by each wave radiated from each individual source and to the side effects created by the coupling phenomena between array source elements. Especially strong coupling phenomena are observed in case of near-field applications where a concentric array of elements is used [4].

The possibility of employing pulsed signals to improve focusing properties has been suggested by various researchers, using as an additional system parameter the time delay between array signals. Although limited information is currently available on the behavior of propagation of pulsed signals with baseband spectral content, the behavior arising from precursor phenomena is expected to be useful in focusing electromagnetic waves.

The propagation of a single pulse inside dispersive dielectric media has received widespread treatment by the use of asymptotic analysis [5], [6], transform techniques [7], time-domain integral equation solvers [8] and the finite-difference time-domain algorithm [9]–[11]. In [12] and [13], a Fourier-series-based methodology is presented and utilized to study the dynamics of short trapezoidally modulated microwave signals inside homogeneous dispersive biological media from the point-of-view of possible hazardous health effects. The Fourier-series approach yields a good approximation for a single pulse when the period of the pulse train is large compared with an individual pulse duration, avoiding the difficulties often encountered in the numerical inversion of the Fourier integral representation due to the highly oscillating nature of the transform kernel [14]. Furthermore, the analysis of the error properties of recent finite-difference-based algorithms for pulse propagation in a dispersive medium suggests that the computational mesh density required to represent precursor signals may become excessive for simulations of realistic problems in two and three dimensions [15]. Almost all these works have been restricted to the propagation of a pulsed electromagnetic plane wave in homogeneous dispersive dielectric media and the main interest has been focused on the study of the associated precursor fields.

Recently, focusing properties of waves emitted from TE_{10} rectangular waveguides inside a layered lossy cylinder have been investigated by using pulse modulated microwave signals [16]. In this paper, an integral-equation technique in conjunction with a Galerkin's procedure are adopted to predict the medium response to time harmonic excitation of the TE_{10} array. The temporal dependence of the field produced at any point within tissue due to single compact incident pulses originating from the array elements is then obtained in the form of an inverse Fourier integral. By employing a high-frequency (9.5 GHz) carrier, the use of a large number of applicators, compared to low-frequency systems, is enabled and focusing at a point of interest within a biological tissue model is achieved by applying time coincidence and constructive phase interference principles. In order to investigate the focusing properties of pulsed baseband signals, sources fed from TEM waveguides could be used. In this direction, the selection of a structure shown in Fig. 1 is a natural selection based on the use of TEM waveguides meeting the above requirements. This is a problem of considerable practical importance due to the recent advances in electromagnetic source technology, which permit the generation of high-peak-power electromagnetic pulse train signals with rapid rise times and short pulse durations [17].

In this paper, the transmission of pulsed baseband signals radiated from a concentric waveguide array in a three-layer cylindrical lossy model is analyzed theoretically. The possibility of using pulsed signals with low-frequency components

Manuscript received March 16, 1998.

The authors are with the Department of Electrical and Computer Engineering, National Technical University of Athens, Zografos 15773, Athens, Greece.

Publisher Item Identifier S 0018-9480(00)00216-7.

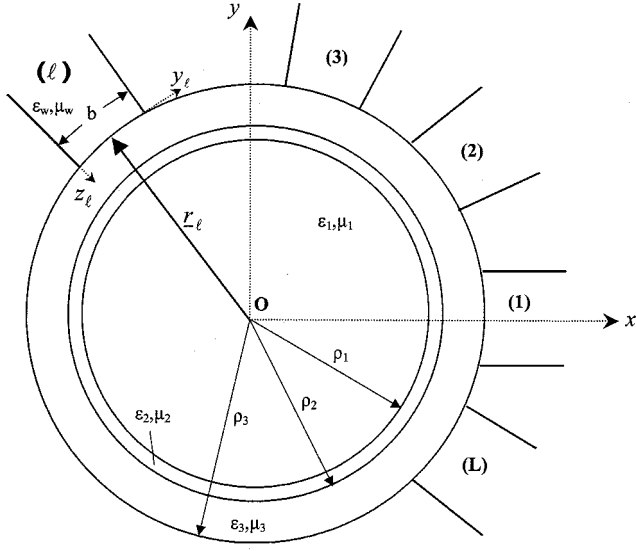


Fig. 1. Three-layer cylindrical model irradiated by a concentric array of TEM waveguide applicators.

and associated increased penetration depth has motivated the initiation of the present study. The proposed method is based on the treatment of individual pulses as members of a pulse train so that the problem is amenable to a Fourier-series analysis. The presented method is applicable to a class of incident signals having periodic time variation

$$\underline{E}_{\text{incident}}(\underline{r}, t) = \underline{E}_{\text{incident}}(\underline{r}, t + T_0) \quad (1)$$

where T_0 is the period of the pulse train. This class of signals has a Fourier-series representation for which each member of the discrete spectrum defines the complex amplitude of a time-harmonic incident wave. The propagation of the incident field to an observation point within the tissue medium is modeled by using an integral-equation technique in order to solve the associated boundary value problem for each spectral component and then a Fourier-series representation is produced for the transmitted wave field. It is important to emphasize that a detailed analysis is employed, which takes into account the modification of the field on each waveguide aperture resulted from the other radiating elements of the array as well as from the presence of the lossy layered dielectric body standing at the near-field region.

The paper is organized as follows. The formulation and analysis for the prediction of the exact field evolution over the entire space-time domain of interest is presented in Section II. In Section III, the necessary checks for the validation of the numerical results are presented, followed by a set of numerical results for a specific tissue-array geometry in Section IV.

II. MATHEMATICAL FORMULATION AND ANALYSIS

The system examined in this paper consists of an arbitrary number (L) of identical parallel-plate waveguide applicators. The geometry of the radiating system looking into a three-layer cylindrical lossy model of circular cross section is shown in Fig. 1. The three layers can be used to simulate different biological media with dispersive characteristics, such as skin, bone, and brain tissues. Alternatively, the two internal layers may be

used to simulate biological media (e.g., brain and bone tissues) with the external layer simulating a lossless dielectric medium, which is commonly used to prevent excessive heating of the tissue surface. The dielectric properties of the layers are denoted with the corresponding frequency-dependent relative complex permittivities $\varepsilon_1(\omega)$, $\varepsilon_2(\omega)$, $\varepsilon_3(\omega)$. The magnetic properties of regions 1–3 are assumed to be independent of frequency and are defined as $\mu_1 = \mu_2 = \mu_3 = \mu_0$, which is appropriate for the simulation of baseband pulse propagation in biological media. The free-space wavenumber is $k_0 = \omega\sqrt{\varepsilon_0\mu_0}$, where ε_0 and μ_0 are the free-space permittivity and permeability, respectively. The applicators are filled with a dielectric material of relative permittivity ε_w and relative permeability μ_w and have an aperture size of b circulating around the cylindrical body's surface while their infinite dimension is parallel to the cylindrical body's axis. It is assumed that the apertures are not completely planar and are conforming to the cylindrical body's surface. Radiating apertures are separated by perfectly conducting flanges. By considering a global cylindrical polar coordinate system ρ , φ , z the position vector of the ℓ th applicator's aperture center is expressed $\underline{r}_\ell = \rho_3\hat{\rho} + \varphi_\ell\hat{\varphi}$, $\ell = 1, 2, \dots, L$. An input pulse signal $g_\ell(t)$, $\ell = 1, 2, \dots, L$ is considered to be driven to the applicators, which is repeated with a period T_0 so that the incident signal can be written as a pulse train as

$$g_{P,\ell}(t) = \bar{\delta}(t) * g_\ell(t) \quad (2)$$

where $\bar{\delta}(t)$ is an infinite sequence of impulse functions, spaced at the pulse repetition interval T_0

$$\bar{\delta}(t) = \sum_{n=-\infty}^{+\infty} \delta(t - nT_0) \quad (3)$$

and $*$ is the convolution operator. The incident pulse train given in (2) has the standard Fourier-series representation

$$g_{P,\ell}(t) = \sum_{n=-\infty}^{+\infty} c_\ell(n) \exp(jn\omega_0 t) \quad (4)$$

with $\omega_0 = 2\pi/T_0$ the pulse train fundamental angular frequency. The complex amplitude of the n th Fourier component is given by

$$c_\ell(n) = \frac{2}{T_0} \int_{-T_0/2}^{T_0/2} g_{P,\ell}(t) \exp(-jn\omega_0 t) dt \quad (5)$$

The strategy of the present approach is to use this Fourier-series representation of the incident pulse train, to analyze the propagation of each Fourier component individually into the structure of interest, by applying the analysis presented in Section II-A, and then to sum the individual transmitted components to reconstruct the propagated response to the pulse train. The pulses in the incident pulse train are assumed to be spaced widely enough apart so that there is no mutual interference of the pulses within the target structure.

A. Time-Harmonic Signals

The analysis begins by considering a single time-harmonic component at a fixed angular frequency $\omega = n\omega_0$. The time

dependence of the field quantities is assumed to be $\exp(+j\omega t)$ and it is suppressed throughout the analysis. In order to solve this boundary value problem, an integral-equation technique is adopted. The solution of the wave equation

$$(\nabla \times \nabla \times - k_0^2 \varepsilon_i \mu_i) \underline{E}_i(\underline{r}) = 0 \quad (6)$$

in cylindrical polar coordinates, inside the tissue layers ($i = 1, 2, 3$) is expressed in terms of cylindrical vector wave functions [18]. Thus,

$$\underline{E}_i(\underline{r}) = \sum_{m=-\infty}^{m=+\infty} \left(a_{im} \underline{M}_{m,k}^{(1)}(\underline{r}, k_i) + b_{im} \underline{N}_{m,k}^{(1)}(\underline{r}, k_i) + a'_{im} \underline{M}_{m,k}^{(2)}(\underline{r}, k_i) + b'_{im} \underline{N}_{m,k}^{(2)}(\underline{r}, k_i) \right) \quad (7)$$

where $k_i = k_0 \sqrt{\varepsilon_i(\omega)}$ and $a_{im}, b_{im}, a'_{im}, b'_{im}$ are to be determined. The cylindrical vector wave functions $\underline{M}_{m,k}^{(q)}(\underline{r}, k_i), \underline{N}_{m,k}^{(q)}(\underline{r}, k_i), q = 1, 2$ are given by [18]

$$\underline{M}_{m,k}^{(q)}(\underline{r}, k_i) = \nabla \times \left(\hat{z} e^{jm\phi} Z_m^{(q)}(k_i \rho) \right) \quad (8)$$

and

$$\underline{N}_{m,k}^{(q)}(\underline{r}, k_i) = \frac{1}{k_i} \nabla \times \underline{M}_{m,k}^{(q)}(\underline{r}, k_i), \quad q = 1, 2. \quad (9)$$

In (8) and (9), ρ, φ are the cylindrical polar coordinates and $Z_m^{(1)}(k_i \rho) = J_m(k_i \rho), Z_m^{(2)}(k_i \rho) = Y_m(k_i \rho)$ are Bessel's and Neumann's functions.

Next, the fields inside the waveguide applicators are described by using the waveguides normal modes. If the operating frequency is lower than the TM_1 cutoff frequency, only a single mode, the TEM mode, with a zero cutoff frequency will be propagating in the waveguides. Thus, the fields inside each waveguide applicator are expressed as the superposition of the incident TEM mode and an infinite number of all the reflected TEM and TM modes since TE modes are not excited due to the geometry of the structure. Thus, the transverse electric field in the ℓ th applicator ($\ell = 1, 2, \dots, L$) can be written, with respect to the local Cartesian coordinates y_ℓ, z_ℓ of the ℓ th waveguide, as follows:

$$\underline{E}_{\ell,t}^w(y_\ell, z_\ell) = A_\ell \underline{e}_t^{EM}(y_\ell) e^{-jkz_\ell} + A'_\ell \underline{e}_t^{EM}(y_\ell) e^{jkz_\ell} + \sum_{m=1}^{\infty} \left[\frac{j\lambda_m}{v_m} B'_{\ell,m} \underline{e}_{m,t}^M(y_\ell) e^{j\lambda_m z_\ell} \right] \quad (10)$$

where

- t the subscript is used to denote the transverse field components;
- A_ℓ complex amplitude of the excited TEM mode in the ℓ th waveguide;
- $A'_\ell, B'_{\ell,m}$ complex amplitudes of the reflected TEM, m th order TM modes, respectively, in the ℓ th waveguide;
- k, λ_m corresponding propagation constants, given by the following equations:

$$k = k_0(\varepsilon_w \mu_w)^{1/2} \quad (11)$$

$$\lambda_m = \left(k_0^2 \varepsilon_w \mu_w - \left(\frac{m\pi}{b} \right)^2 \right)^{1/2}. \quad (12)$$

The transverse \underline{e}_t^{EM} and $\underline{e}_{m,t}^M$ modal fields are [18]

$$\underline{e}_t^{EM}(y_\ell) = \hat{y}_\ell \quad (13)$$

$$\underline{e}_{m,t}^M(y_\ell) = \hat{y}_\ell \sqrt{\frac{2}{b}} \cos\left(\frac{m\pi}{b} y_\ell\right). \quad (14)$$

By satisfying the continuity of the tangential electric- and magnetic-field components on the $\rho = \rho_1$ and $\rho = \rho_2$ interfaces and on the $\rho = \rho_3$ contact surface between cylindrical lossy model and radiating apertures, the following system of L coupled integral equations is obtained in terms of an unknown transverse electric field \underline{E}_α on the waveguide apertures

$$\sum_{q=1}^L \int_{\Gamma_q} \underline{K}_{\ell q}(y/y') \underline{E}_\alpha(y') dy' = 2A_\ell \left(\frac{k}{\omega \mu_0 \mu_w} \right) \underline{h}_t^{EM}(y), \quad \ell = 1, 2, \dots, L \quad (15)$$

where \underline{h}_t^{EM} is the incident TEM mode transverse magnetic field on the aperture of the ℓ th waveguide, and the kernel matrices $\underline{K}_{\ell q}(y/y'), \ell = 1, \dots, L/q = 1, \dots, L$ indicate the effect of coupling from the q th aperture ($y' \in \Gamma_q$) to the ℓ th aperture ($y \in \Gamma_\ell$) and are given in the Appendix. In order to determine the electric field on the waveguide apertures, the system of integral equations (15) is solved. To this end, a Galerkin's technique is adopted by expanding the unknown transverse electric field on each aperture $\underline{E}_{q,a}$ into waveguide normal modes. Therefore, with respect to the q th ($q = 1, 2, \dots, L$) aperture's local Cartesian coordinate system, the electric field on the same aperture is expressed in the following form:

$$\underline{E}_{q,a} = \sum_{m=1}^{\infty} (g_q \underline{e}_t^{EM} + f_{q,m} \underline{e}_{m,t}^M), \quad q = 1, 2, \dots, L. \quad (16)$$

By substituting (16) into the system of coupled integral equations (15), and making use of the waveguide modes orthogonality [18], the system of integral equations (15) is converted into an infinite system of linear equations. Assuming the g_q and $f_{q,m}$ expansion coefficients are determined approximately, the aperture fields can be determined approximately by using (16) and then the coefficients $a_{im}, b_{im}, a'_{im}, b'_{im}$ ($i = 1, 2, 3$) are determined easily. Substituting the values of these coefficients into (7), the electric field at any point inside tissue can be easily computed.

B. Gaussian Pulsed Signals

In this study, a Gaussian pulse train is considered to be driven to the applicators. One period of the time variation of the incident signal of the ℓ th applicator is written as

$$g_\ell(t) = \exp\left(-\frac{\pi(t-t_\ell)^2}{\tau^2}\right), \quad \ell = 1, 2, \dots, L \quad (17)$$

which is centered around the time $t_\ell > 0$, with τ a constant related to the pulsewidth in time. The associated pulse train has a Fourier series representation, according to (4), for which each

member of the discrete spectrum $c_\ell(n)$ defines the complex amplitude of a time-harmonic wave incident to the applicator and is given by

$$c_\ell(n) = \frac{\tau}{T_0} \exp\left(-\frac{n^2\omega_0^2\tau^2}{4\pi}\right) \exp(-jn\omega_0 t_\ell). \quad (18)$$

The incident wave distribution on the waveguide apertures is obtained as a spectrum of TEM components

$$\underline{E}_{\ell, t(\text{incid})}^w(y_\ell, z_\ell = 0; n) = p_\ell c_\ell(n) \underline{c}_t^{EM}(y_\ell) \quad (19)$$

where p_ℓ is the amplitude of the incident TEM mode driven to the ℓ th applicator and $\underline{c}_t^{EM}(y_\ell)$ is the TEM field distribution on the aperture. The quantity of primary interest in this analysis is the complex transfer function $\underline{F}_\ell(\underline{r}; \omega)$, $\ell = 1, 2, \dots, L$ and specifically the discrete spectrum components $\underline{F}_\ell(\underline{r}; n\omega_0) = \underline{F}_\ell(\underline{r}; n)$, representing the field produced at point \underline{r} inside tissue, when only the ℓ th applicator is excited and the field on its aperture is a continuous time-harmonic field ($\exp(+jn\omega_0 t)$) of unit amplitude [$A_\ell = 1$ in (10)]. In computing this field, by using the analysis presented in Section II-A, the power coupling to the remaining applicators of the configuration is taken into account.

It is important to observe that the transfer function $\underline{F}_\ell(\underline{r}; n)$, $\ell = 1, 2, \dots, L$ depends on the relative position of the point of interest $\underline{r} = (\rho, \varphi)$ with respect to the ℓ th applicator. Therefore, the transfer function at a point of interest for each applicator can be computed by exciting only one applicator and then computing the field at different points within tissue, corresponding to the different relative positions of the point of interest with respect to each individual applicator. This is

$$\begin{aligned} \underline{F}_\ell(\underline{r}; n) &= \underline{F}(\underline{r} - \underline{r}_\ell; n) \\ &= \underline{F}(\rho, \phi - \phi_\ell; n), \quad \ell = 1, 2, \dots, L. \end{aligned} \quad (20)$$

The field transmitted from the applicators of the array at the point of interest, at the frequency $\omega = n\omega_0$, is obtained by the following summation over the L elements of the array:

$$\underline{E}(\underline{r}; n) = \sum_{\ell=1}^L p_\ell c_\ell(n) \underline{F}_\ell(\underline{r}; n) \quad (21)$$

The time-domain representation for the total electric field at an observation point within the biological tissue medium is obtained by summing the contributions made by each transmitted frequency component

$$\underline{E}(\underline{r}; t) = \text{Re} \left\{ \sum_{n=1}^N \left(\sum_{\ell=1}^L p_\ell c_\ell(n) \underline{F}_\ell(\underline{r}; n) \right) \exp(jn\omega_0 t) \right\} \quad (22)$$

where $\text{Re}(\cdot)$ denotes the real part of the complex exponential form of the time-domain representation of each transmitted frequency component and N is the mode number of the highest frequency component retained for the Fourier series.

III. VALIDATION OF THE NUMERICAL RESULTS

The method developed here has been applied to investigate the focusing ability of a concentric array consisting of eight

TABLE I
CONVERGENCE FOR THE TEM SELF REFLECTION AND MUTUAL COUPLING COEFFICIENTS $S_{\ell 1} = A'_\ell/A_1$, $\ell = 1, 2, 5$ [SEE (10)] AT $f = 1$ GHz BY INCREASING THE APERTURE MODE NUMBER

| Modes appearing on the excited aperture | S_{11} | S_{21} | S_{51} |
|--|------------------------|-----------------------|------------------------|
| TEM | 0.773 \angle 124° | 0.133 \angle 356.9° | 0.0070 \angle 245.6° |
| TEM, TM ₁ | 0.724 \angle 120.9° | 0.129 \angle 354.6° | 0.0089 \angle 263° |
| TEM, TM ₁ , TM ₂ | 0.714 \angle 117.9° | 0.102 \angle 348.6° | 0.0088 \angle 264.8° |
| TEM, TM ₁ , TM ₂ , TM ₃ | 0.711 \angle 117.3° | 0.101 \angle 348.4° | 0.0089 \angle 265.3° |
| TEM, TM ₁ , TM ₂ , TM ₃ , TM ₄ | 0.708 \angle 116.8° | 0.100 \angle 347.3° | 0.0088 \angle 262.7° |
| TEM, TM ₁ , TM ₂ , TM ₃ , TM ₄ , TM ₅ | 0.7078 \angle 116.7° | 0.100 \angle 347.1° | 0.0090 \angle 263.1° |

TEM waveguides, at a point of interest inside a two-layer cylindrical biological tissue model, 16 cm in diameter, surrounded by a lossless dielectric layer. The two layers of the biological tissue model are used to simulate bone and brain tissues. The thicknesses of the bone and the external dielectric layers are taken to be $\rho_2 - \rho_1 = 0.5$ cm and $\rho_3 - \rho_2 = 2$ cm, respectively ($2\rho_3 = 20$ cm). The dielectric constant of the external layer used in the calculations is $\epsilon_3 = 2.1$. In order to obtain the complex relative permittivities of the tissue media, available literature data points [19] for dielectric constant and conductivity of bone and brain tissues have been used and interpolated values have been computed at any frequency. However, more elaborate relaxation models can also be used to obtain the frequency-dependent permittivity of biological media [20]. The applicators aperture size is defined by $b = 7.5$ cm. The aperture centers are placed symmetrically at the periphery of the external dielectric layer and the corresponding position vectors are $\underline{r}_\ell = 10(\text{cm})\hat{\rho} + \varphi_\ell\hat{\varphi}$, $\ell = 1, 2, \dots, 8$, with $\varphi_1 = 0^\circ$, $\varphi_2 = 45^\circ$, \dots , $\varphi_8 = 315^\circ$.

The input signal driven to each applicator is considered to be a Gaussian pulse train, with an individual pulse duration of $\tau = 1$ ns, and with a pulse repetition interval of $T_0 = 10$ ns.

In order to check the developed numerical code, several trials have been performed. In the first place, the computation of the transfer function, by using the analysis presented in Section II-A, has been checked. Regarding the numerical evaluation of the kernel matrix elements $\underline{K}_{\ell q}(y/y')$ given in the Appendix, the infinite summation with respect to the order m of Bessel's functions in the expression of fields inside the tissue layers [(7)] is computed, by truncating as high as $m \sim 30$.

The convergence and stability of the solution in the frequency domain have been examined by increasing the number of modes included in the aperture electric fields $\underline{E}_{q, a}$ [(16)]. In Table I, convergence patterns are presented, in terms of the coefficients A'_ℓ of (10), when only applicator 1 is excited by a time-harmonic field of unit amplitude ($A_1 = 1$ in (10)) at $f = 1$ GHz. These coefficients correspond to the self-reflection coefficient ($S_{11} = A'_1$) and the mutual coupling coefficients between neighboring ($S_{21} = A'_2$) and opposite ($S_{51} = A'_5$) applicators of the examined configuration. From Table I, it can be easily observed, that the subset of modes (TEM, TM₁, TM₂, TM₃, TM₄) appearing on applicator apertures is sufficient to assure convergence of the solution. Furthermore, the continuity of the tangential fields at the $\rho = \rho_1$ and $\rho = \rho_2$ interface planes between different layers has been checked and verified numerically, while the validity of the boundary conditions

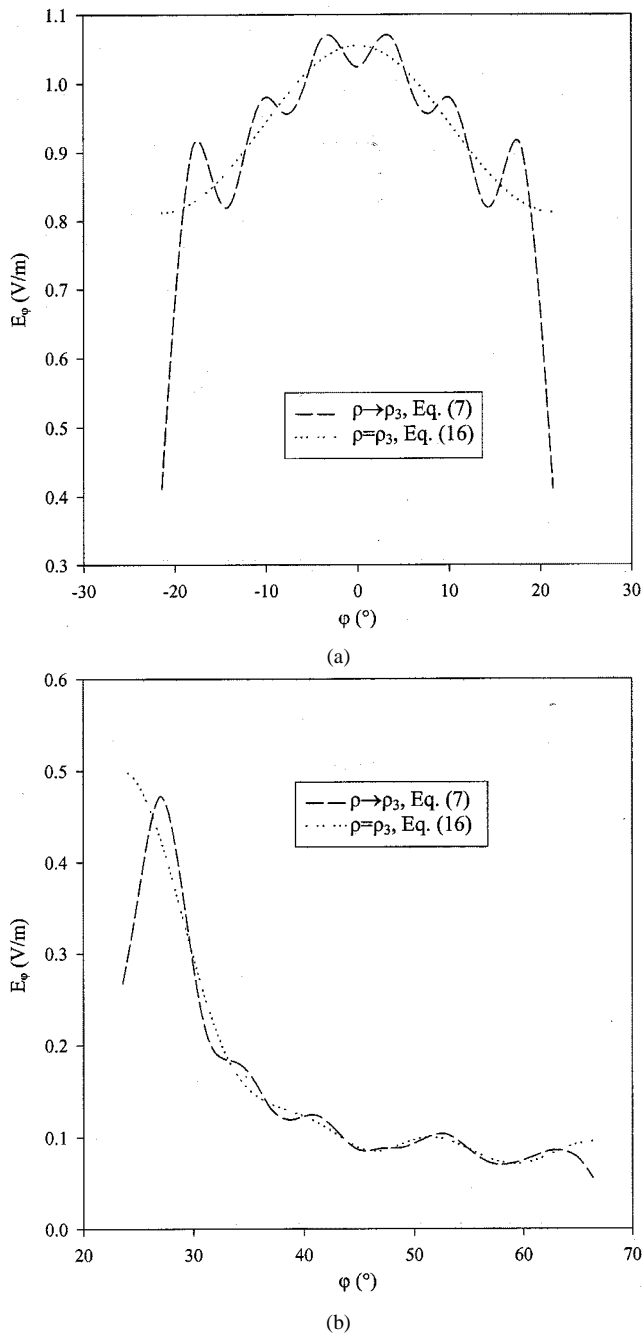


Fig. 2. A two-layer tissue model, 16 cm in diameter, simulating bone and brain tissues, surrounded by a 2-cm-thick lossless dielectric layer, is irradiated by a symmetric concentric array of eight waveguides with $b = 7.5$ cm. Field distributions: (a) on aperture (1) and (b) on aperture (2), when only applicator (1) is excited by a time-harmonic field of unit amplitude at 1 GHz. Comparison of the results of (7) and (16).

on the $\rho = \rho_3$ interface has also been checked. In Fig. 2, the electric-field distributions on the waveguide apertures 1 and 2 are presented, when only applicator 1 is excited by a time-harmonic field of unit amplitude [$A_1 = 1$ in (10)] at $f = 1$ GHz. The aperture electric field intensities, computed directly from the series of (7) are compared with the results of (16) for the field inside region 3 when $\rho \rightarrow \rho_3$. As it is known, the Galerkin technique employed in Section II-A satisfies the boundary conditions on the $\rho = \rho_3$ surface approximately. This is exhibited in Fig. 2. Notice that at the waveguide apertures

edges, the well-known Gibbs phenomenon [21] associated with the Fourier series is observed.

It is important to emphasize the fact that the developed analysis takes into account the effects on each aperture field from the other radiating elements and from the layered dielectric cylinder standing at the near-field region. The exact knowledge of the electric field at the apertures permits the evaluation of the electric field inside tissue with high precision.

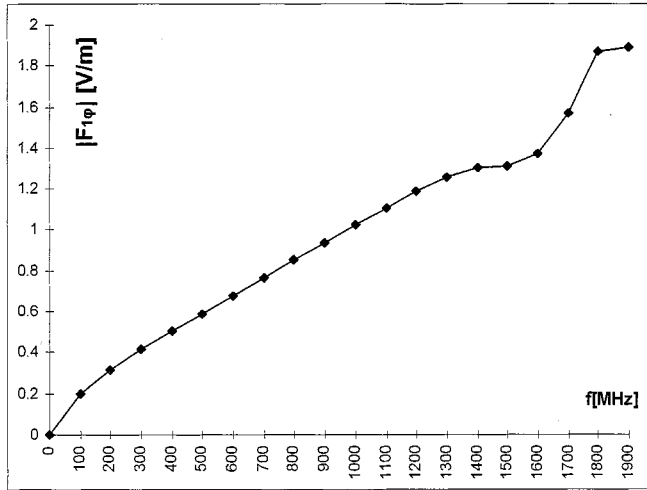
IV. NUMERICAL RESULTS AND DISCUSSION

Numerical computations have been performed for the geometry described in Section III. First, by using the analysis presented in Section II-A, the discrete n th-order component of the complex transfer function $\underline{F}(\rho, \varphi - \varphi_\ell; n)$, $\ell = 1, 2, \dots, L/n = 1, 2, \dots, N$ at any point inside the cylindrical model can be computed. In Fig. 3(a)–(f), the magnitude of the main (φ) component of the transfer function is shown at different points on the axis of radiating aperture 1, inside the dielectric layer and the tissue media, over the frequency bandwidth of the used signals ($f < f_0$, f_0 being the cutoff frequency of the TM_1 mode). On the surface of the dielectric layer, the amplitude of the transfer function increases with increasing frequency, reaching its maximum value at the high edge of the frequency spectrum, where the transmitted power from the waveguide into the dielectric becomes larger and, thus, the waveguide radiation more effective.

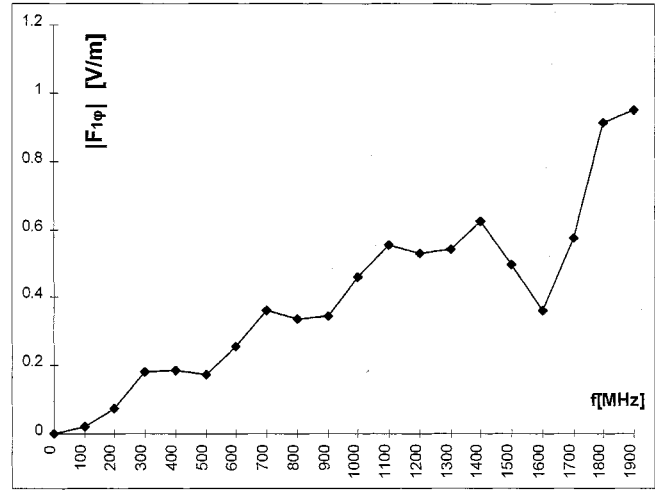
As the pulse proceeds deeper into the lossy model, the amplitudes of the individual frequency components decay in different rates with distance and the contribution of low-frequency components becomes more pronounced with increasing depth. The difference between the transfer function at the high (1900 MHz) and low (100 MHz) frequency edge is of the order of 15 dB at the bone-brain interface, while at 3-cm depth from the tissue surface, a 10-dB difference is observed.

Selective resonance phenomena are observed near 400, 700, 1100, and 1400 MHz, while the maximum value of the transfer function is reached at the high edge of the frequency spectrum. At the bone-brain interface, the resonance at 1400 MHz is 4.5 dB stronger than the corresponding resonance at 400 MHz, but as the propagation distance increases, the relative importance is changed, and at 3-cm depth from the tissue surface a 2.5-dB difference is observed.

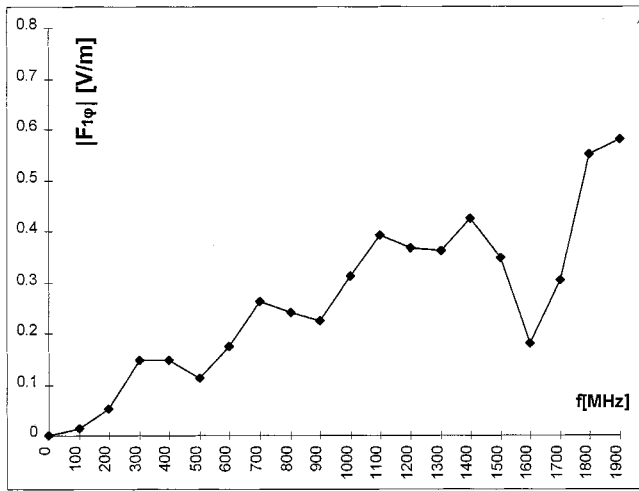
The time-domain waveforms at the same points along the axis of applicator 1 can then be computed by using (22) and are presented in Fig. 4(a)–(f), when only applicator 1 is excited ($p_1 = 1$, $p_2 = \dots = p_8 = 0$, and $t_1 = 0$). The waveform in Fig. 4(a) was computed at a position immediately following the contact surface between aperture 1 and the external dielectric layer at the aperture center, while in Fig. 4(b)–(f), the temporal evolution of the pulsed fields propagating inside the tissue layers along the axis of applicator 1 is shown. A 70% decrease in the peak amplitude of the pulse is observed after the 2-cm propagation distance inside the external dielectric layer, while a 25% decrease is observed for the 0.5-cm propagation inside bone layer, a 5% decrease for the first 0.5-cm propagation inside brain tissue and a 30% decrease for the next 2-cm propagation inside brain. Secondary peaks appearing in the obtained waveforms, which



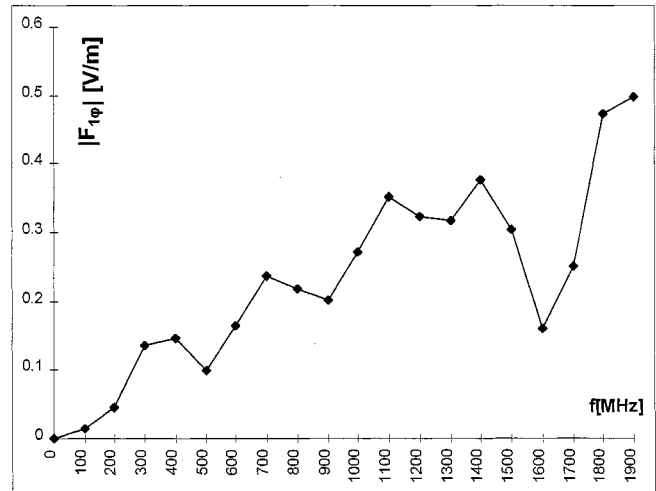
(a)



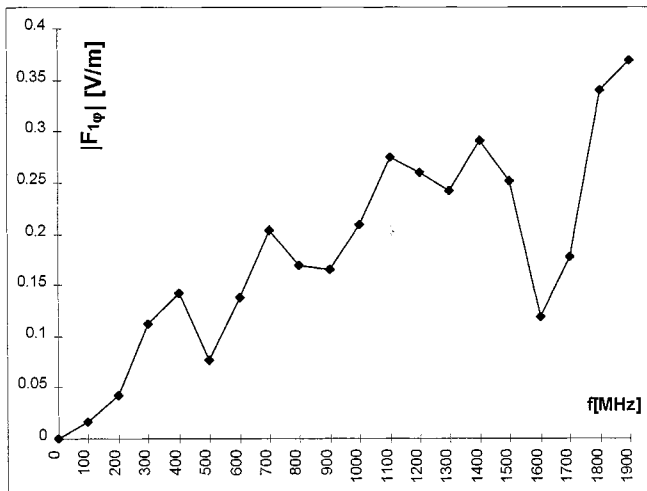
(b)



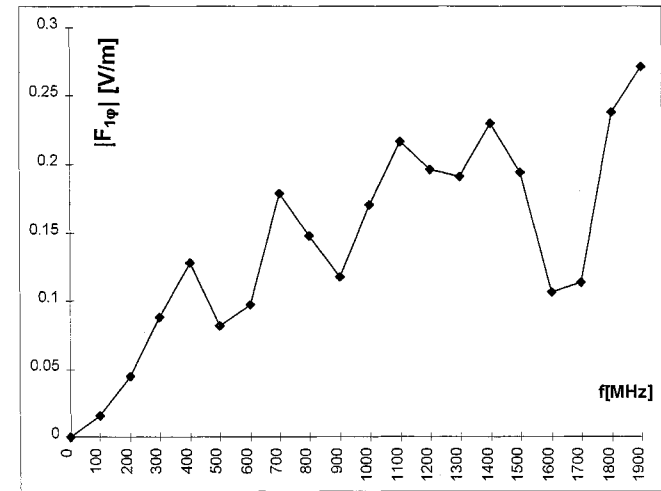
(c)



(d)



(e)



(f)

Fig. 3. Magnitude of the main component ($|F_{1\phi}|$) of the transfer function at several positions on the axis of radiating aperture 1 for the same tissue-array geometry considered in Fig. 2. The input signals driven to the individual applicators are assumed to be Gaussian pulse trains with initial 1-ns pulsewidth and a pulse repetition rate of 10 ns. The transfer function is computed for uniform array excitation. (a) On the surface of the dielectric layer. (b) On the interface between dielectric and bone layers. (c) On the interface between bone and brain layers. (d) At 1-cm propagation distance inside tissue. (e) At 2-cm propagation distance inside tissue. (f) At 3-cm propagation distance inside tissue.

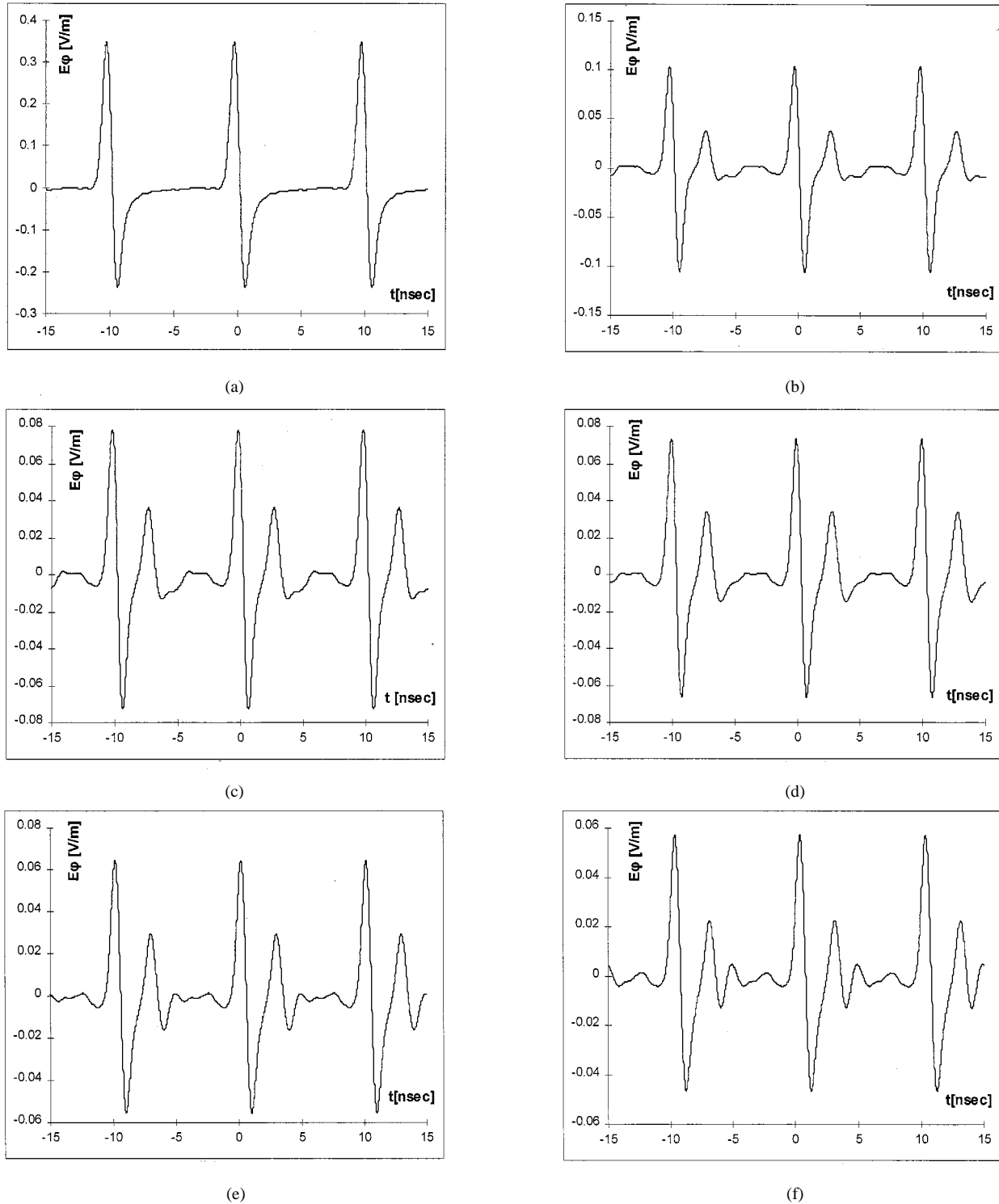


Fig. 4. Temporal evolution of the main component (E_ϕ) of the field along the axis of aperture 1, when only this applicator is excited with unit amplitude. (a) On the surface of the external dielectric layer. (b) On the surface of the bone layer. (c) At the interface between bone and brain tissues. (d) At 1-cm propagation distance inside tissue. (e) At 2-cm propagation distance inside tissue. (f) At 3-cm propagation distance inside tissue.

are comparable in strength with the main peak of the pulse, can be explained by considering the power coupling through the apertures of the array and the scattering phenomena occurring in the examined geometry.

In an attempt to focus the electromagnetic radiation at a point of interest $\underline{r} = 6\hat{\rho}$ (cm) within the brain tissue, located at 2-cm depth from the tissue surface on the axis of applicator 1, time

coincidence of the fields originated from the eight waveguides of the array is used. To this end, the discrete spectrum components of the transfer function of each individual applicator are computed and the temporal evolution of the main vector component E_ϕ of the field originated from each individual applicator at the point of interest is examined in detail in Fig. 4(e) and Fig. 5. Due to the x -axis symmetry and to the fact that the

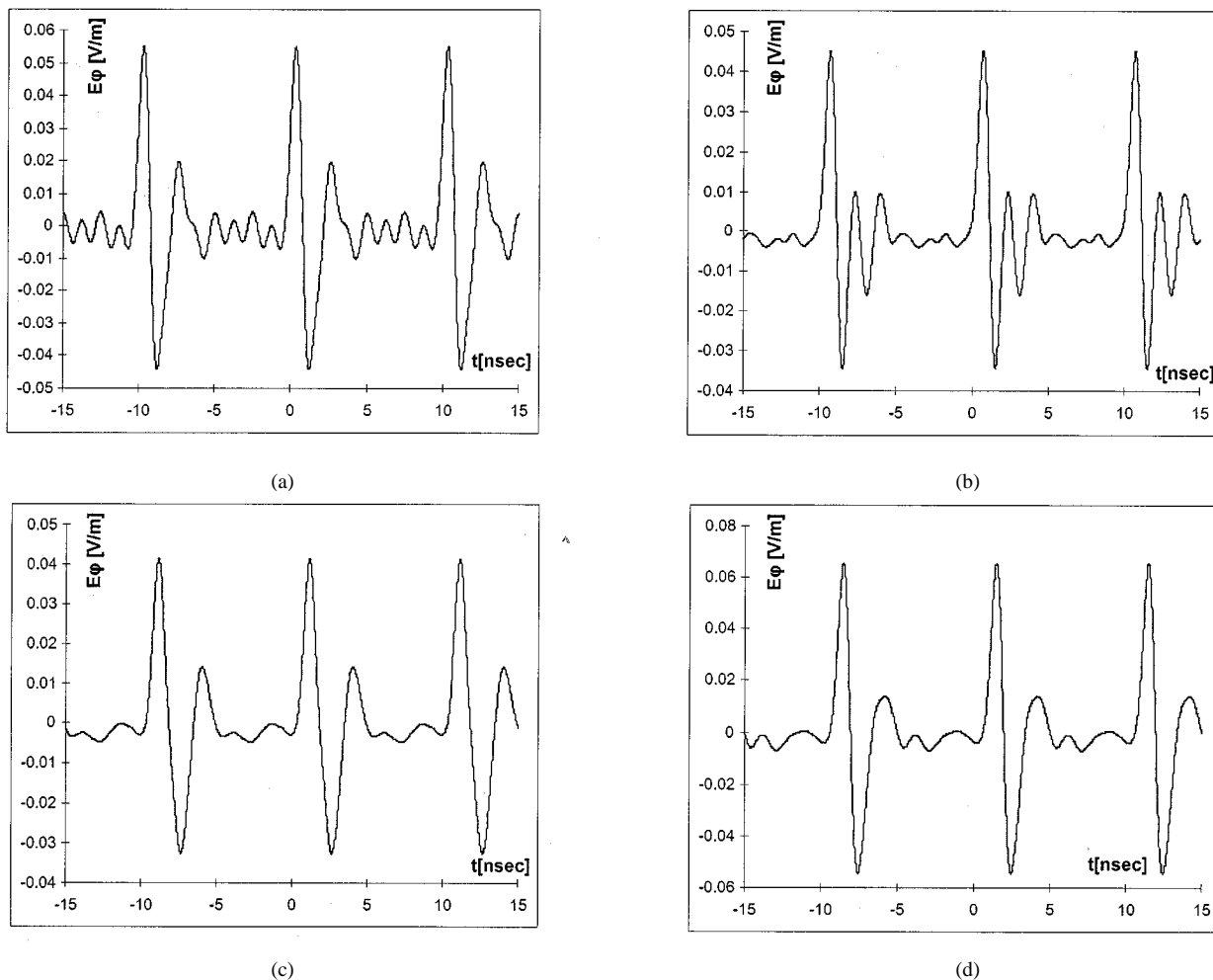


Fig. 5. Temporal evolution of the main component (E_φ) of the field produced at a point of interest, located at 2-cm depth inside tissue, on the axis of applicator 1, when only one applicator of the array is excited. (a)–(d) Successive excitation of applicators 2–5.

axes of applicators 1 and 5 coincide to the x -axis, only the fields produced from applicators 1 to 5 of the array are presented in Fig. 4(e) and Fig. 5(a)–(d), respectively. It can be observed that the main contribution is from the most neighboring to the point of interest array elements (applicators 1 and 2). Furthermore, it is important to note the significant contribution from the array opposite element (applicator 5).

The time dependence of the field produced at the point of interest is shown in Fig. 6(a) for uniform array excitation ($p_1 = \dots = p_8 = 1$, $t_1 = \dots = t_8 = 0$) and in Fig. 6(b) for the following type of excitation:

$$\begin{aligned} p_1 &= p_2 = p_3 = p_4 = p_5 = p_6 = p_7 = p_8 = 1 \\ t_1 &= 0.14 \text{ ns} \\ t_2 &= t_8 = 0.29 \text{ ns} \\ t_3 &= t_7 = 0.70 \text{ ns} \\ t_4 &= t_6 = 1.14 \text{ ns} \\ t_5 &= 1.46 \text{ ns} \end{aligned}$$

which has been selected to achieve time coincidence of the signals at the point of interest.

By comparing Fig. 6(a) with Fig. 6(b), a 100% increase of the main peak amplitude of the pulse is achieved by adjusting the

excitation of the pulsed signals driven to the individual applicators. Moreover, by integrating the squared magnitude of the electric field for a period of $T_0 = 10$ ns, it can be easily observed that a 340% increase of the deposited power at the point of interest is achieved by adjusting the array temporal excitation.

V. CONCLUSION

A rigorous analysis has been presented for predicting the electromagnetic field produced in a layered cylindrical lossy model by an array of concentrically placed TEM waveguide applicators excited by pulsed signals with baseband spectral content. Numerical results have been computed and presented for a bone–brain tissue model irradiated by an eight-element array, by considering as input signal to each individual applicator, a Gaussian pulse train with short pulsewidth (~ 1 ns) and sufficiently large repetition interval (10 ns). By adjusting the time delay of the signals injected to the individual applicators, focusing at a target point within brain tissue has been achieved. These results provide an enhanced physical insight of pulse propagation inside layered lossy media and can be used in order to achieve focusing inside biological tissues.

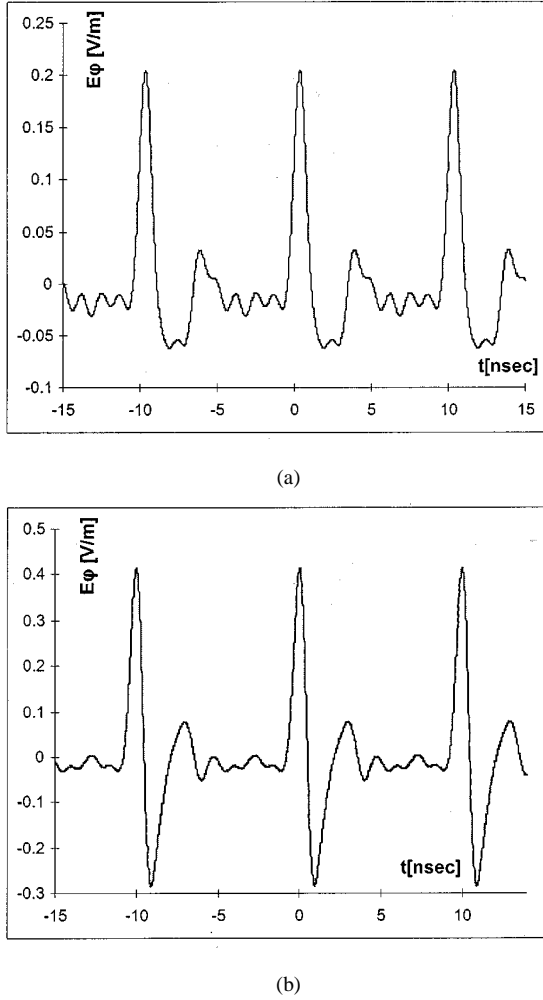


Fig. 6. Temporal evolution of the main field component (E_φ) at the point of interest. (a) For uniform array excitation. (b) For array excitation adjusted to achieve focusing.

APPENDIX

KERNEL MATRIX FUNCTIONS $\overline{K}_{\ell q}(y/y')$

$$\begin{aligned} \overline{K}_{\ell q}(y/y') &= \sum_{m=-\infty}^{+\infty} e^{jm(\varphi_\ell - \varphi_q)} \exp \left[jm \left(-\frac{y}{\rho_3} \right) + \left(\frac{y'}{\rho_3} \right) \right] \overline{N}(m) \\ &\quad - \delta_{\ell q} \overline{\Omega}(y/y'), \quad \ell = 1, 2, \dots, L; q = 1, 2, \dots, L \end{aligned} \quad (\text{A.1})$$

where $\delta_{\ell q}$ is the Kronecker's delta

$$\begin{aligned} \overline{\Omega}(y/y') &= \left(\frac{k}{b\omega\mu_0\mu_w} \right) \underline{h}_t^{EM} \underline{e}_t^{EM} \\ &\quad + \sum_{n=1}^{\infty} \left\{ \left(\frac{\omega\varepsilon_0\varepsilon_w}{\lambda_n} \right) \underline{h}_n^M, t \underline{e}_n^M, t \right\} \end{aligned} \quad (\text{A.2})$$

and

$$\overline{N}(m) = \frac{j}{2\pi\omega\mu_0\rho_3} \overline{L}'(m; \rho_3) \left(\overline{L}(m; \rho_3) \right)^{-1}. \quad (\text{A.3})$$

The matrices involved in (A.3) are given by the following equations:

$$\overline{L}'(m; \rho) = \overline{T}_{3m}^{(1)}(\rho) + \frac{Z_m^{(2)}(k_3\rho)}{Z_m^{(1)}(k_3\rho)} \overline{T}_{3m}^{(2)}(\rho) \overline{R}_{3m} \quad (\text{A.4})$$

$$\overline{L}(m; \rho) = \overline{D}_{3m}^{(1)}(\rho) + \frac{Z_m^{(2)}(k_3\rho)}{Z_m^{(1)}(k_3\rho)} \overline{D}_{3m}^{(2)}(\rho) \overline{R}_{3m} \quad (\text{A.5})$$

where

$$\overline{D}_{im}^{(q)}(\rho) = \begin{pmatrix} -\frac{\partial Z_m^{(q)}(k_i\rho)/\partial\rho}{Z_m^{(q)}(k_i\rho)} & 0 \\ 0 & k_i \end{pmatrix}, \quad i = 3/q = 1, 2 \quad (\text{A.6})$$

and

$$\begin{aligned} \overline{T}_{im}^{(q)}(\rho) &= \begin{pmatrix} 0 & -k_i \frac{\partial Z_m^{(q)}(\alpha_i\rho)/\partial\rho}{Z_m^{(q)}(\alpha_i\rho)} \\ k_i^2 & 0 \end{pmatrix}, \quad i = 3/q = 1, 2 \end{aligned} \quad (\text{A.7})$$

with

$$Z_m^{(1)}(k_i\rho) = J_m(k_i\rho) \text{ and } Z_m^{(2)}(k_i\rho) = Y_m(k_i\rho) \quad (\text{A.8})$$

being Bessel's or Neuman's functions, respectively, and

$$\begin{aligned} \overline{R}_{3m} &= \frac{Z_m^{(1)}(k_3\rho)}{Z_m^{(2)}(k_3\rho)} \left(\overline{T}_{3m}^{(2)} - \overline{G}_{2m} \overline{F}_{2m} \overline{D}_{3m}^{(2)} \right)^{-1} \\ &\quad \cdot \left(-\overline{T}_{3m}^{(1)} + \overline{G}_{2m} \overline{F}_{2m} \overline{D}_{3m}^{(1)} \right), \quad \text{at } \rho = \rho_2. \end{aligned} \quad (\text{A.9})$$

The matrices involved in (A.9) are

$$\overline{G}_{2m}(\rho) = \overline{T}_{2m}^{(1)} + \frac{Z_m^{(2)}(k_2\rho)}{Z_m^{(1)}(k_2\rho)} \overline{T}_{2m}^{(2)} \overline{R}_{2m} \quad (\text{A.10})$$

and

$$\overline{F}_{2m}(\rho) = \left[\overline{D}_{2m}^{(1)} + \frac{Z_m^{(2)}(k_2\rho)}{Z_m^{(1)}(k_2\rho)} \overline{D}_{2m}^{(2)} \overline{R}_{2m} \right]^{-1}. \quad (\text{A.11})$$

The matrices $\overline{D}_{im}^{(q)}$, $\overline{T}_{im}^{(q)}$, $i = 1, 2$ and $q = 1, 2$ appearing in (A.11) are obtained from (A.6) and (A.7), respectively, for $i = 1, 2$.

REFERENCES

- [1] J. Chen and O. P. Gandhi, "Numerical simulation of annular phased arrays of dipoles for hyperthermia of deep seated tumors," *IEEE Trans. Biomed. Eng.*, vol. 39, pp. 209–216, Mar. 1992.
- [2] K. S. Nikita, N. G. Maratos, and N. K. Uzunoglu, "Optimal steady-state temperature distribution for a phased array hyperthermia system," *IEEE Trans. Biomed. Eng.*, vol. 40, pp. 1299–1306, Dec. 1993.
- [3] A. Boag, Y. Leviatan, and A. Boag, "Analysis and optimization of waveguide multiapplicator hyperthermia systems," *IEEE Trans. Biomed. Eng.*, vol. 40, pp. 946–952, Sept. 1993.
- [4] K. S. Nikita and N. K. Uzunoglu, "Coupling phenomena in concentric multiapplicator phased array hyperthermia systems," *IEEE Trans. Microwave Theory Tech.*, vol. 44, pp. 65–74, Jan. 1996.
- [5] K. E. Oughstun and J. E. K. Laurens, "Asymptotic description of electromagnetic pulse propagation in a linear causally dispersive medium," *Radio Sci.*, vol. 26, pp. 245–258, 1991.
- [6] K. E. Oughstun and G. C. Sherman, "Uniform asymptotic description of ultrashort rectangular optical pulse propagation in a linear, causally dispersive medium," *Phys. Rev. A: Gen. Phys.*, vol. 41, pp. 6090–6113, 1990.
- [7] P. Wyns, D. P. Fotty, and K. E. Oughstun, "Numerical analysis of the precursor fields in linear dispersive pulse propagation," *J. Opt. Soc. Amer. A: Opt. Image Sci.*, vol. 6, pp. 1421–1429, 1989.

[8] J. Bolomey, C. Durix, and D. Lesselier, "Time domain integral equation approach for inhomogeneous and dispersive slab problems," *IEEE Trans. Antennas Propagat.*, vol. AP-26, pp. 658–667, Sept. 1978.

[9] R. Joseph, S. Hagness, and A. Taflov, "Direct time integration of Maxwell's equations in linear dispersive media with absorption for scattering and propagation of femtosecond electromagnetic pulses," *Opt. Lett.*, vol. 16, pp. 1412–1414, 1991.

[10] R. J. Luebbers and F. Hunsberger, "FD-TD for n -th order dispersive media," *IEEE Trans. Antennas Propag.*, vol. 40, pp. 1297–1301, Nov. 1992.

[11] P. G. Petropoulos, "The wave hierarchy for propagation in relaxing dielectrics," *Wave Motion*, vol. 21, pp. 253–262, 1995.

[12] R. Albanese, J. Penn, and R. Medina, "Short-rise-time microwave pulse propagation through dispersive biological media," *J. Opt. Soc. Amer. A: Opt. Image Sci.*, vol. 6, pp. 1441–1446, 1989.

[13] J. G. Blashank and J. Frazen, "Precursor propagation in dispersive media from short-rise-time pulses at oblique incidence," *J. Opt. Soc. Amer. A: Opt. Image Sci.*, vol. 12, pp. 1501–1512, 1995.

[14] W. C. Chew, *Waves and Fields in Inhomogeneous Media*, New York: Van Nostrand, 1990.

[15] P. G. Petropoulos, "Stability and phase error analysis of FD-TD in dispersive dielectrics," *IEEE Trans. Antennas Propagat.*, vol. 42, pp. 62–69, Jan. 1994.

[16] K. S. Nikita and N. K. Uzunoglu, "Analysis of focusing of pulse modulated microwave signals inside a tissue medium," *IEEE Trans. Microwave Theory Tech.*, vol. 44, pp. 1788–1798, Oct. 1996.

[17] J. Benford and J. Swengle, *High Power Microwaves*. Norwood, MA: Artech House, 1992.

[18] D. S. Jones, *Theory of Electromagnetism*, New York: Pergamon, 1964.

[19] H. P. Schwan and K. R. Foster, "RF field interactions with biological systems: Electrical properties and biophysical mechanism," *Proc. IEEE*, vol. 68, pp. 104–113, Jan. 1980.

[20] C. Gabriel, S. Gabriel, and E. Corthout, "The dielectric properties of biological tissues," *Med. Phys.*, vol. 41, pp. 2231–2293, 1996.

[21] R. V. Churchill, *Fourier Series and Boundary Value Problems*, New York: McGraw-Hill, 1941.



Konstantina S. Nikita (M'96) received the Diploma in electrical engineering and the Ph.D. degree from the National Technical University of Athens, Athens, Greece, in 1986 and 1990, respectively, and the M.D. degree from the Medical School, University of Athens, in 1993.

Since 1990, she has been a Researcher in the Institute of Communication and Computer Systems, National Technical University of Athens. In 1996, she joined the Department of Electrical and Computer Engineering, National Technical University

of Athens, where she is currently an Assistant Professor. She has been the Technical Manager of a number of European and National Research and Development projects in the field of biomedical engineering. Her current research interests include applications of electromagnetic waves in medicine, electromagnetic scattering, diffraction topography, medical imaging and image processing, nonlinear optimization algorithms, and applications.

Dr. Nikita is a member of the Technical Chamber of Greece, the Athens Medical Association, and the Hellenic Society of Biomedical Engineering.

Georgios D. Mitsis was born in Ioannina, Greece, on February 5, 1975. He received the Diploma in electrical and computer engineering from the National Technical University of Athens, Athens, Greece, in 1997, and is currently working toward the M.S. degree in electrical engineering and the Ph.D. degree in biomedical engineering at the University of Southern California.

His main research interests are in the areas of nonlinear and nonstationary system identification and modeling with applications to biological systems and also in biomedical effects of microwaves.



Nikolaos K. Uzunoglu (M'82–SM'97) was born in Constantinople, in 1951. He received the B.Sc. degree in electronics from the Technical University of Istanbul, Istanbul, in 1973, and the M.Sc. and Ph.D. degrees from the University of Essex, Essex, U.K., in 1974 and 1976, respectively, and the D.Sc. degree from the National Technical University of Athens, Athens, Greece, in 1981.

From 1977 to 1984, he was a Research Scientist in the Office of Research and Technology, Hellenic Navy. In 1984, he was elected Associate Professor in the Department of Electrical Engineering, National Technical University of Athens, and in 1987, he became a Professor. In 1986, he was elected Vice-Chairman of the Department of Electrical Engineering, National Technical University of Athens, and in 1988, he was elected Chairman of the same department. He was reelected as Chairman in 1990 and 1992 twice. In 1991, he was elected and appointed Director of the Institute of Communication and Computer Systems, an independent research establishment associated with the National Technical University of Athens. He served in this position until 1999. He has authored or co-authored over 120 publications in refereed international journals, and has published three books in Greek on microwaves, fiber optics telecommunications, and radar systems. His research interests include electromagnetic scattering, propagation of electromagnetic waves, fiber optics telecommunications, and high-speed circuits operating at gigabit/second rates.

Dr. Uzunoglu has been the National Representative of Greece to the COST, Technical Telecommunications Committee, actively participating in several COST telecommunications projects since 1988. He has also been Project Manager of several RACE, ESPRIT, ACTS and National Research and Development Projects in the fields of telecommunications and biomedical engineering applications. He was the recipient of the 1981 International G. Marconi Award in Telecommunications. In 1994, he was elected an Honorary Professor of the State Engineering University of Armenia. He was awarded the honorary Ph.D. diploma from the Universities of Bucharest, Cluj-Napoca, and Orade. In 1998, he was elected Foreign Member of the National Academy of Sciences of Armenia.